DEVELOPMENT AND APPLICATION OF AN INVERSE BUILDING MODEL FOR DEMAND RESPONSE IN SMALL COMMERCIAL BUILDINGS

Kyoung-ho Lee and James E. Braun
Ray W. Herrick Laboratories, School of Mechanical Engineering
Purdue University, West Lafayette, IN
leekh@ecn.purdue.edu and jbraun@ecn.purdue.edu

ABSTRACT

This paper describes development of an inverse building model and its application in studying the performance of a demand-limiting (DL) control strategy. The demand-limiting strategy involves precooling (PC) a building during unoccupied times, maintaining the zone temperature setpoints at the lower limit of comfort during off-peak, occupied periods, and then limiting the peak cooling rate to a target for on-peak, occupied times that keeps zone conditions within comfort limits. Data from the Iowa Energy Center (IEC), which is typical of small commercial buildings, were used to train an inverse model that was then employed as a tool to evaluate the potential for peak load reduction through control of building thermal mass. The potential for demand limiting was investigated through parametric analysis compared with night-setup (NS) control.

INTRODUCTION

In small commercial buildings, the control of dedicated HVAC equipment is achieved through the use of a thermostat, which allows the setting of zone temperature set points. Most HVAC systems employ a strategy called night-setup control. Under night-setup control, the air temperatures are in the middle of the comfort range during occupied times and the cooling system is typically inactive during unoccupied periods.

Recently there has been increased interest in the development of setpoint adjustment strategies that utilize building thermal mass to perform load shifting and peak load reduction (Braun (1990), Kintner-Meyer and Emery (1995), Keeney and Braun (1996), Keeney and Braun (1997), Braun et al. (2001), Chaturvedi and Braun (2002), Henze et al. (2004)). These strategies typically involve precooling during unoccupied periods and raising of setpoints during occupied, on-peak periods.

Transient building models are useful in the development and evaluation of strategies that take advantage of building thermal mass. Building models can be categorized as forward or inverse models. Forward models use a physical description of the building, whereas inverse models are trained using on-site measurements. Forward models are necessary for design, whereas inverse models can be useful for developing site-specific control strategies.

There has been a lot of work on the development of simplified inverse building models. Recently, Chaturvedi and Braun (2002) developed an inverse gray-box building model that was applied by Braun et al. (2002) to develop and evaluate load-shifting strategies for a large commercial building. The model uses a simplified physical representation with a thermal network of resistors and capacitors. The network is transformed to a transfer function representation and used to predict the cooling loads. The resistors and capacitors are learned using a training algorithm that minimizes model prediction errors for the overall cooling load. The model was tested using data from a field site in Chicago and was able to predict cooling loads to within about 9% for a four-week test period.

Gouda et al. (2002) also suggested a lumped parameter building model based on a thermal network. Parameters for the wall models were estimated by nonlinear constrained optimization using Kuhn-Tucker equations. Free-floating simulation results for internal air temperatures for low and high capacity rooms based on 2nd-order walls were compared with measured data.

The work described in the current paper involved further development, evaluation, and application of the inverse building model presented by Chaturvedi and Braun (2002). An inverse model was developed and applied to the

Energy Resource Station (ERS) building at the Iowa Energy Center (IEC) for the purpose of evaluating demand-limiting building thermal mass control strategies. The IEC ERS building is a relatively lightweight structure that is representative of small commercial buildings and is very well instrumented for model validation and control strategy evaluations. Recently, the International Energy Agency (IEA) reported an empirical validation of forward building models, TRNSYS, PROMETHEUS, DOE, and IDA-ICE, for the IEC ERS building (Travesi et al. (2001)).

The model trained with data from the ERS was used to estimate peak cooling load reduction associated with different demand-limiting and precooling strategies. Parametric analyses were conducted to understand the impact of the control parameters on demand-limiting performance.

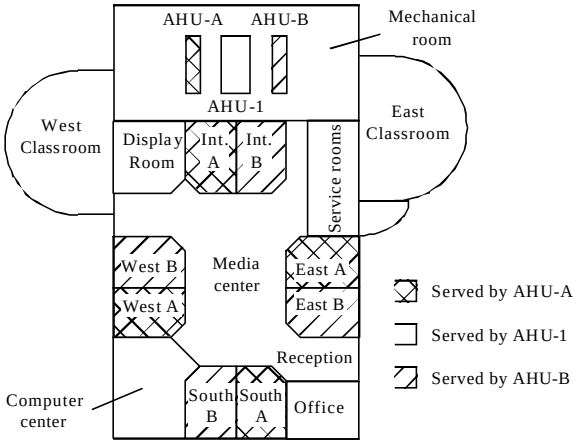

Figure 1 Schematic diagram of floor plan for the ERS

DESCRIPTIONS OF TEST BUILDING

The Iowa Energy Center ERS building is typical of small commercial buildings that employ packaged air conditioning equipment. It is a single-story building having a slab floor and is located in Ankeny, Iowa (Price and Smith (2000)). The ERS is a demonstration and test facility built to compare different energy-efficient measures, to record energy consumption, and to disseminate information concerning energy-efficient design and operation of buildings. A schematic diagram of the floor plan for the ERS is shown in Figure 1.

The ERS is divided into three major areas: the general area and two sets of test rooms, designated A and B. Each set of test rooms is comprised of East, South, West, and interior rooms. The general area consists of office space, a display room, a computer center, two classrooms, service rooms, a media center, a reception space, and a mechanical room. Each test room has 274.97 ft^2 of floor area and the ceiling is 8.5 ft high. The height of plenum zones above the test zones is 5.5 ft. The test room zones within a pair are identical and labeled 'A' and 'B'.

The IEC ERS was previously used to demonstrate the potential for load shifting associated with a simple building thermal mass precooling strategy (Braun et al. (2002)). Data from these tests were used in the current study to train inverse models. For the testing, uniform control strategies were applied to the entire facility for two different phases. In the first phase of testing (Phase 1), night-setup control was applied for the entire facility over a 9-day period. A set point of 74^{o}F was specified during the occupied period (7 a.m. to 6 p.m.) and a set point of 80^{o}F was used for the unoccupied period (6 p.m. to 7 a.m.). For the second test (Phase 2), the entire building was run with a simple precooling strategy for 8 days. The daytime cooling set point was 74 ^{o}F from 6 a.m. to 6 p.m.. Then, the temperature was setup to 80 ^{o}F from 6 p.m. to midnight. The precooling temperature set point was 68^{o}F from midnight to 6 a.m.. Internal gains within each zone were simulated using baseboard heat and lights between 7 a.m. to 6 p.m. for the entire duration of both phases. No blinds were used in the test rooms. There is an on-site weather station that recorded measurements of outdoor dry bulb, relative humidity, wind speed and direction, normal solar flux, and global horizontal solar flux during the testing period. Measurements for each zone included air flow rate, supply air temperature, return air temperature, and reheat power input. Zone sensible cooling requirements were estimated from these measurements. Data were hourly averaged.

DEVELOPMENT OF INVERSE BUILDING MODEL

Inverse building model

Figure 2 shows a thermal network for a simplified building model of the ERS. All test zones involving West, East, South, and interior rooms were modeled as a single zone enclosed by external walls, internal walls, the roof and the floor with multiple walls being lumped together as a single wall. Thus, in this study, cooling loads of the ERS building represent a total cooling load for the combined test rooms. This combination is representative of a small commercial building.

Each of the walls uses two capacitors to represent the mass of the walls and three resistors to represent the wall coupling to the ambient, the conduction within the wall and the wall coupling to the zone. It is assumed that solar radiation through windows is absorbed only on the floor. Since internal radiation is due to lights located on the ceiling, internal radiative gains are distributed only to the walls and floor. Infiltration and radiation between building outside surface and night sky are neglected. The temperature in the adjacent zone, T_{zo}, is assumed to be equal to T_z.

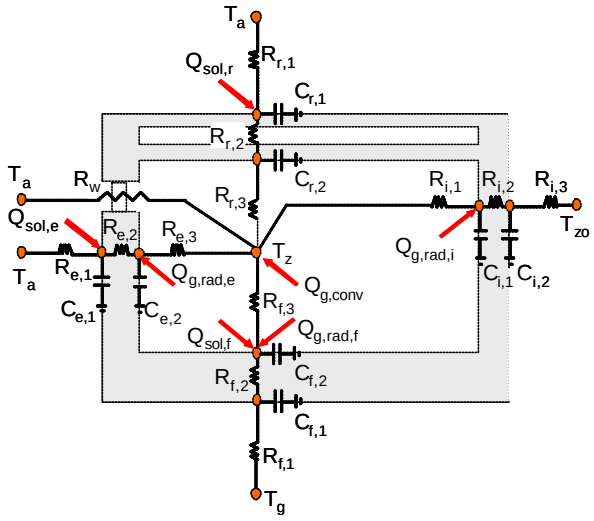

Figure 2 Thermal network for inverse building model

Using an energy balance at each node, a state-space formulation was set up for the building model as described by Chaturvedi and Braun (2002).

$$\frac{d\mathbf{x}_b}{dt} = \mathbf{A}_b\mathbf{x}_b + \mathbf{B}_b\mathbf{u}_b \tag{1}$$

$$\mathbf{Y}_b = Q_b = \mathbf{C}_b\mathbf{x}_b + \mathbf{D}_b\mathbf{u}_b \tag{2}$$

where Q_b = rate of instantaneous heat gain to the building air. The state and input vectors in the above representation are

$$\mathbf{x}_b^T = [T_{r1}, T_{r2}, T_{e1}, T_{e2}, T_{f1}, T_{f2}, T_{i1}, T_{i2}] \tag{3}$$

$$\mathbf{u}_b^T = [T_z, T_a, T_g, Q_{sol,r}, Q_{sol,e}, Q_{g,rad,f}, Q_{g,rad,e}, Q_{g,rad,i}, Q_{sol,f}, Q_{g,conv}] \tag{4}$$

There are 8 state variables (two nodal temperatures in each of the four walls) and 10 input variables in the model. Measured zone temperature, ambient temperature, solar radiation, internal radiative gains, and internal convective gains are used for input variables. Ground temperature is assumed constant. The ground temperature was estimated using experimental results from Thomas and Rees (1999) and Zhou et al. (2002) that give an estimated steady-

state floor surface heat flux of 5 W/m^{2}K. The ground temperature was estimated to be 63.5°F. It is also assumed that the internal radiative gains are distributed within an even heat flux to the interior surfaces of the walls and floor. It was assumed that 90% of the lighting energy was radiation and 10% was convection. For the heaters, 5% was assumed to be radiation and 95% convection. The elements of the coefficient matrices in the state space representation are in terms of the resistors and capacitors used in the different walls. The state-space representation is then solved using the methodology of Seem et al.(1989) to obtain a comprehensive transfer function for heat gain in terms of the input variables and previous heat gains as:

$$Q_{b,k} = \left(\sum_{j=0}^{N_{\mathbf{x}}} \mathbf{S}_{b,j} \mathbf{u}_{b,k-j} \right) - \left(\sum_{j=1}^{N_{\mathbf{x}}} e_{b,j} Q_{b,k-j} \right) \quad (5)$$

$S_{b,j}$ and $e_{b,j}$ are determined from the matrices $\mathbf{A}_b, \mathbf{B}_b, \mathbf{C}_b$, and $\mathbf{D}_b$ involving resisters and capacitors. Further solution details are found in Seem et al. (1989). The instantaneous sensible zone cooling load $Q_{c,k}$ can be calculated using an instantaneous energy balance on the zone given as:

$$C_{z,eff} \frac{dT_{z,k}}{dt} = Q_{b,k} - Q_{c,k} \quad (6)$$

The zone temperature is assumed to vary linearly, so that the left-hand-side of equation 6 is expressed as:

$$\frac{dT_{z,k}}{dt} = \frac{T_{z,k} - T_{z,k-1}}{\Delta t} \quad (7)$$

where $\Delta t = 1$ hour. From equation 5, $Q_{b,k}$ is expressed as a function of the instantaneous zone temperature. However, for computational simplicity, it is assumed that the average heat gains and average cooling rate are constant throughout the hour and are evaluated at the average temperature over the hour and the variation in set point is linear over the hour.

The training algorithm is divided into two phases, a global search and a local search (Chaturvedi and Braun (2002)). The global search uses a systematic search to determine reasonable values of the building resistors and capacitors. It uses initial parameter estimates obtained from a crude building description to appropriately bound the parameters and searches within the bounded region. The local search uses a local non-linear regression method to further improve the R and C estimates by minimizing the root-mean-squared error between measured and calculated cooling loads for the training duration. The combination of a local and a global phase provides a robust algorithm for determining an accurate model and only requires minimal preliminary building information. Parameters determined through global and local searches are: effective window transmittance for solar radiation, effective zone capacitance, and the thermal resistances and capacitances shown in Figure 2. Effective zone capacitance appears in equation 6 and effective transmittance is used to calculate solar gains through windows.

Tables 1 and 2 give the bounds used for the global search in the model training for the ERS building.

Table 1 Material property bounds used in model training algorithm

PROPERTY	BOUNDS	ELEMENT TYPE			
		EXTERNAL WALL	INTERNAL WALL	ROOF AND CEILING	FLOOR
k_t (Btu/hr-F-ft)	Min	1E-3	1E-3	1E-5	1E-3
	Max	1.0	1.0	5E3	1.0
$r * C_p$ (Btu/F-ft^3)	Min	0.1	0.1	0.1	0.1
	Max	30	10	50	30

Table 2 Physical property bounds used in model training algorithm

BOUNDS	τ_{eff}	h_i (Btu/hr-ft^2-F)	h_e (Btu/hr-ft^2-F)	$C_{z,eff}$ (Btu/F)
Min	0.1	0.1	2.0	0
Max	0.9	1.0	6.0	800

Table 3 Cases of data sets for testing performance

DATA SET CASES	TRAINING	TESTING
I	phase 1 (9 days)	phase 2 (8 days)
II	phase 2 (8 days)	phase 1 (9 days)
III	first 6 days of phase 1 + phase 2 (14 days)	repetition of last 3 days of phase 1 (9 days)
IV	phase 1 + first 5 days of phase 2 (14 days)	repetition of last 3 days of phase 2 (9 days)

The trained model can be used to calculate transient building cooling loads for arbitrary periods if the inputs are provided.

Validation of model

The measured data sets for the phase 1 (9 days from August 3 to August 11, 2001) and phase 2 (8 days from August 13 to August 20, 2001) tests at the ERS building were used as inputs to the inverse building model. A part of the data was used for training the model and the remainder was used for testing the model. Table 3 represents four cases that were considered for training and testing of the inverse model. In cases of III and IV, portions of data from both phase 1 and phase 2 were used for training. In each of these cases, only 3 days of data were not used for training and these 3 days were repeated 3 times in sequence to obtain 9-day test sequences.

Model performance is described in terms of a prediction error, E_{rms}, as defined in equation 8.

$$E_{\text{rms}}(\%) = \frac{100}{Q_{\text{m,max}}}\sqrt{\frac{\sum_{k=1}^{N_{\text{test}}}(Q_{\text{m,k}} - Q_{\text{c,k}})^2}{N_{\text{test}} - 1}} \tag{8}$$

Testing performance of the inverse model for the four cases is shown in Figure 3. The bars represent errors for model testing given for the entire test period ('Whole period') and the last 3 days of the test data ('Last 3 days'). Generally the model performs well in estimating cooling loads compared with measured cooling loads. The E_{rms} values were within 8% except for the case of training with phase 2 and testing with phase 1 data, which had about a 12% error. A better model could be obtained if more data were available over a wider range of conditions. For the remainder of the results presented in this paper, a model was used that was trained using all of the data from the phase 1 and phase 2 testing. This model resulted in an E_{rms} of 6.22% for the training data set.

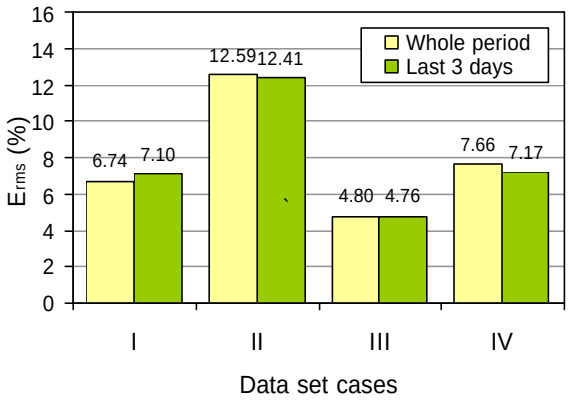

Figure 3 E_{rms} of inverse model with 4 cases of training and testing data sets

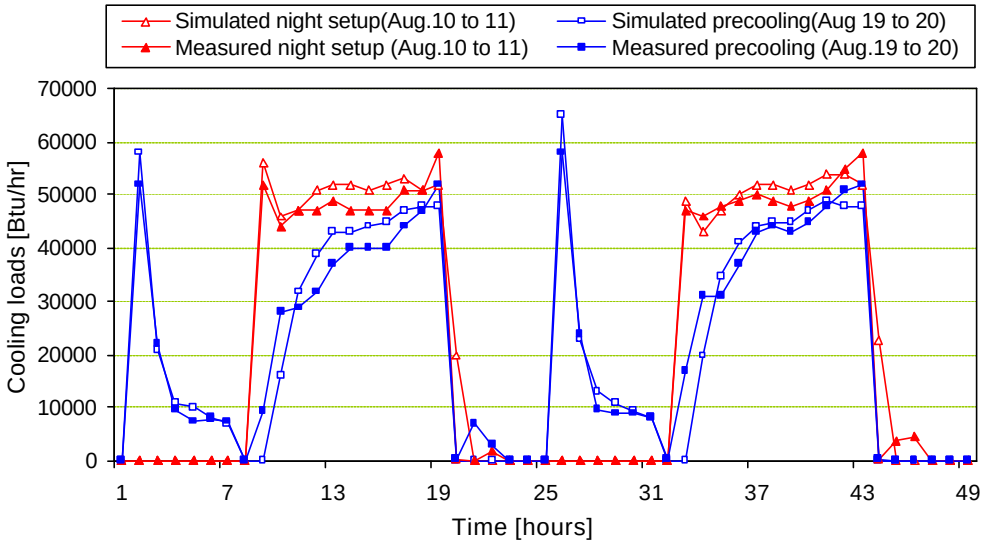

Figure 4 Comparison of measured and simulated cooling loads (inverse model) for night-setup and precooling control strategies

Figure 4 compares the calculated and measured cooling loads for two days of the phase 1 and phase 2 test periods obtained using the model trained with all available data. These two days had similar solar radiation and ambient temperature conditions. Therefore, the cooling loads shown in Figure 4 are useful for evaluating the impact of precooling on load shifting as well as evaluating model performance. The simulated cooling load matches the actual cooling loads very well. For both simulated and measured results, the occupied period load was about 23% less for the precooling tests and the peak load was reduced by about 9%.

The precooling control strategy used for the phase 2 testing was not designed to maximize peak load reduction. Much greater peak load reductions would be possible if the zone temperatures were varied within the comfort region rather than being held constant. Such a strategy would keep the zone temperatures low at the beginning of occupancy and raise them later in the day. This would have the effect of increasing the early occupancy loads and decreasing the late occupancy loads. The impact of such a demand-limiting strategy on peak loads was evaluated using the inverse model developed in this study for the ERS. Results are presented in the next section.

APPLICATION OF INVERSE BUILDING MODEL

Demand-limiting strategy

A demand-limiting (DL) control strategy in this study is defined as a strategy that aims to "limit" the peak cooling load to a specified target cooling load during the on-peak period by adjusting room set point temperatures within the comfort range. Figure 5 represents set point temperatures for both night setup (NS) and DL control strategies. In the DL strategy, the building is precooled by lowering the set point to $T_{dl,unoc}$ (e.g., 67°F) during a portion of the unoccupied period leading up to the occupied time.

During the occupied period, the set point is set at the lower end of the comfort limit at $T_{dl,oc,min}$ (e.g., 69°F) until the cooling load would exceed a certain target demand-limiting cooling load. When the building cooling load would exceed the target load, the set point temperature is increased in order to limit the building cooling load to the target load. After the occupied period, the setpoints are set up to $T_{ns,unoc}$ (e.g., 80°F) until the start of the next precooling period.

In this study, the target load was adjusted each day through iteration so as to utilize the entire comfort range. The secant method was used to determine the target load that would yield a zone temperature at the end of the occupied period of $T_{dl,oc,max}$ (76°F).

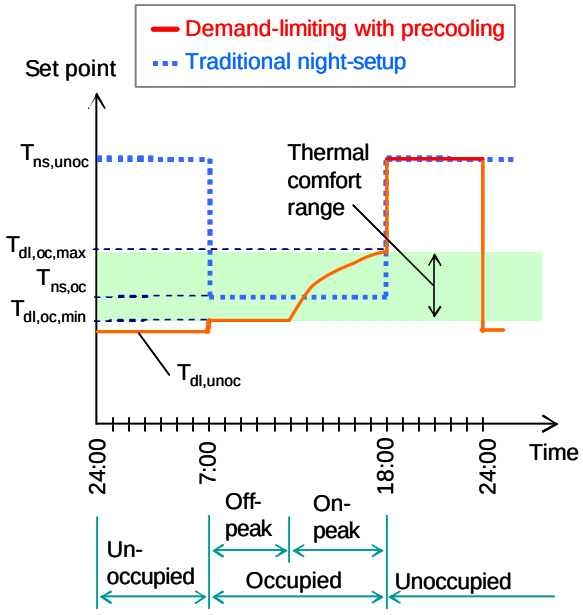

Figure 5 Set point temperatures for night-setup and demand-limiting strategies

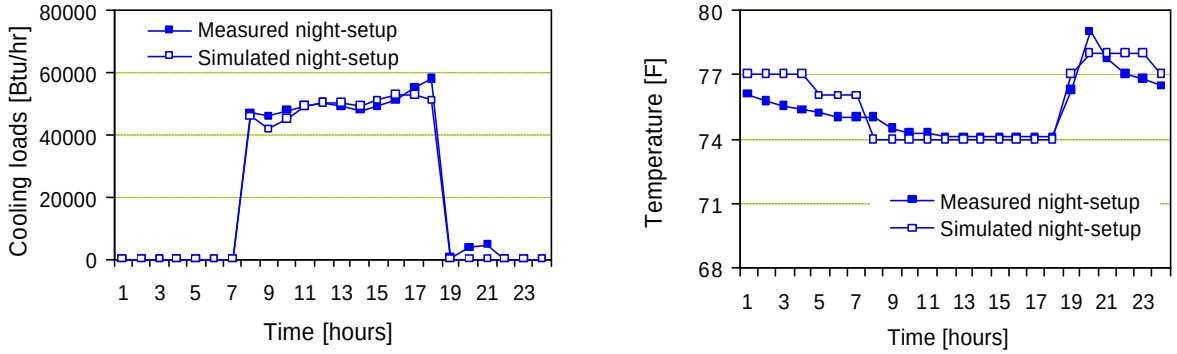

(a) Cooling loads *(b) Zone temperatures*

Figure 6 Measured and simulated (inverse model) cooling loads for night-setup operation on August 11 test in Phase 1

Description of parametric studies

In order to evaluate the potential for the DL control strategy, one day from the phase 1 (Aug. 11) testing was chosen for comparison with a base case of NS control. Every simulation was conducted for an identical set of ten days in a row to erase the initial condition effects and reach a steady-periodic behavior. Figure 6 shows how well the inverse model estimates cooling loads and zone temperatures for this single day under NS. The times are measured from midnight. Cooling loads occurred from 7 a.m. to 6 p.m.. The model did a good job of calculating the cooling loads under NS control.

The demand-limiting period, or on-peak period where the DL strategy is applied, was varied by changing the start-time (DL start time) from 7 a.m. to 3 p.m.. The precooling period was also changed by varying the start-time (H_{pc}) from 10 p.m. to 7a.m.. A start-time of 7 a.m. for precooling represents no precooling during the unoccupied period and is a limiting case. Other setpoints that impact peak loads for the DL and NS strategies were also considered. Table 4 shows the range of parameters considered in this study.

Table 4 Parameter variations

PARAMETERS	VALUES
DL start time	7 a.m. to 3 p.m.
H_{pc}	10 p.m. to 7 a.m.
$T_{dl,oc,min}$(^oF)	67, 69, 71, 73 °F
$T_{dl,unoc}$ (^oF)	63, 65, 67, 69 °F
$T_{dl,oc,max}$ (^oF)	74, 76, 78, 80 °F
$T_{ns,oc}$ (^oF)	72, 74, 76, 78, 80 °F
$T_{ns,unoc}$ (^oF)	80 °F

The performance of the DL strategy was measured in terms of a peak load ratio (*PLR*) defined as the ratio of the peak load under the DL strategy to the peak load for the base case NS strategy or

$$PLR = \frac{Q_{max,dl,op}}{Q_{max,ns,op(@T_{ns,oc}=74°F)}} \tag{9}$$

The base case NS strategy had an unoccupied setpoint ($T_{ns,unoc}$) of 80°F and an occupied setpoint of ($T_{ns,oc}$) of 74°F.

For NS control, the impact of the occupied setpoint on demand was also considered. In this case, a peak load ratio under NS (PLR_{ns}) is defined as

$$PLR_{ns} = \frac{Q_{max,ns,op@T_{ns,oc}}}{Q_{max,ns,op(@T_{ns,oc}=74°F)}} \tag{10}$$

Results and discussion

The effects of start times for demand limiting and night precooling on peak cooling load reduction are shown in Figure 7. The temperature set points for these results are $T_{dl,unoc}$=67°F, $T_{dl,oc,min}$=69°F, $T_{dl,oc,max}$=76°F, and $T_{ns,unoc}$=80°F. PLR has a small dependence on the precooling duration (H_{pc}) when the demand-limiting period begins in the afternoon. However, precooling becomes more important as the start of the on-peak period moves earlier in the day. For an on-peak period beginning at 7 a.m., the maximum peak load reduction was about 23% compared to NS control. For an afternoon start to the on-peak period, the peak load reduction for the on-peak period was about 40% even without any precooling.

Figures 8 and 9 show selected detailed results from the cases considered for Figure 7. These figures compare hourly cooling loads and zone temperatures for the NS and DL strategies for a morning and afternoon start to the demand-limiting period. For the results of Figure 8, the DL strategy involved precooling the building from midnight to 7 a.m. and demand-limiting began at 7 a.m.. The peak load under NS occurred around 5 p.m. in the afternoon. As a result of precooling, the DL strategy resulted in very low loads during the early morning hours. When the load reached the target, then the setpoint was raised following a trajectory that kept the load constant. The zone temperature set point increased until it reached 76 °F at the end of the on-peak period.

For the results of Figure 9, the start time for demand limiting was 1 p.m. As a result, the setpoint was kept low during the morning hours for the DL strategy and the late morning loads were slightly greater than those for the NS control. With a short demand-limiting period, the peak reduction was significantly greater than for the results of Figure 8. The energy storage is more significant compared to the total load for a shorter demand-limiting period. Although not shown here, the application of DL control without precooling results in a significant early morning load spike that occurrs at the start of the occupied period.

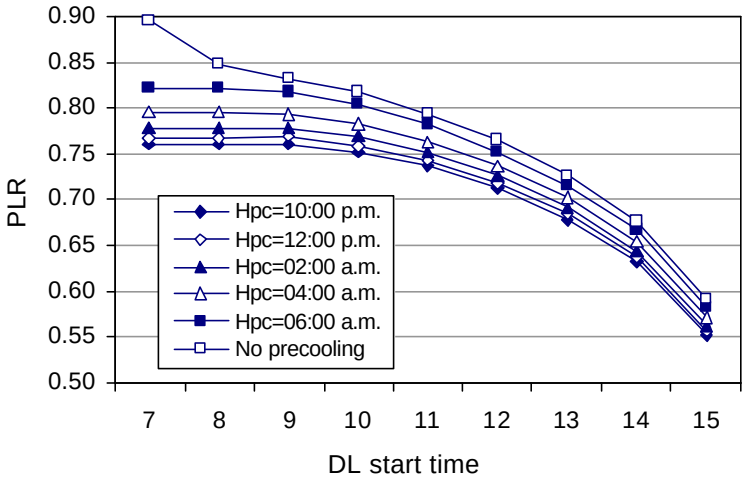

Figure 7 PLR with H_{pc} varying DL start time

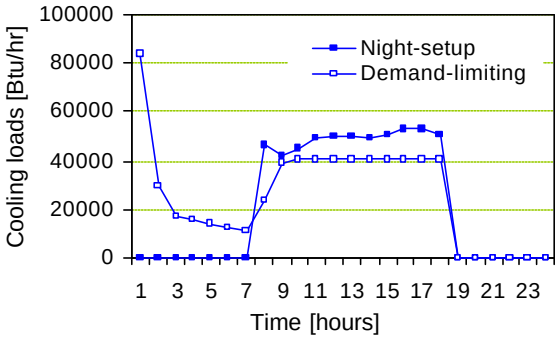

(a) Cooling loads

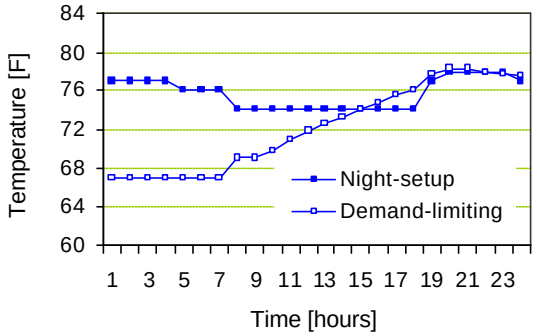

(b) Zone temperatures

Figure 8 Simulated NS and DL control (PC start-time (H_{pc}) of midnight and DL start-time of 7 a.m.)

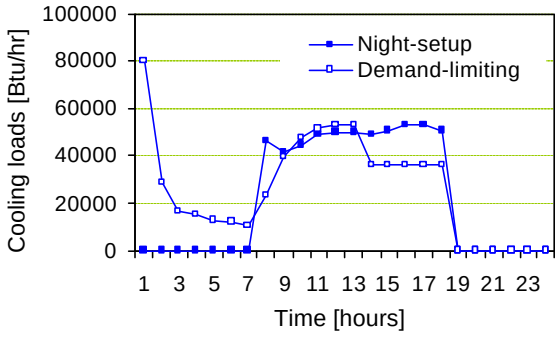

(a) Cooling loads

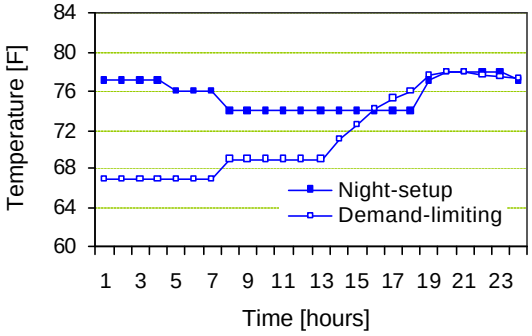

(b) Zone temperatures

Figure 9 Simulated NS and DL control (PC start-time (H_{pc}) of midnight and DL start-time of 1 p.m.)

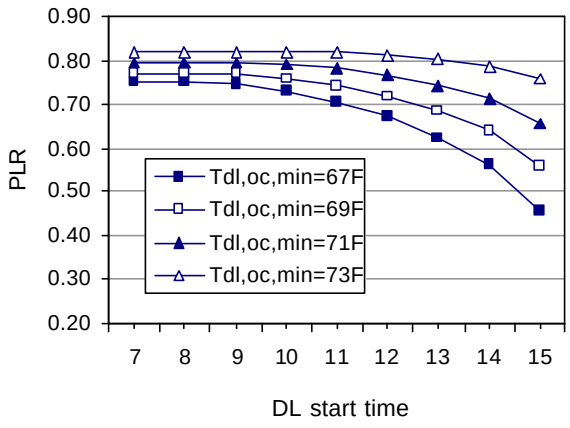

Figure 10 PLR dependence on $T_{dl,oc,min}$ and DL start time

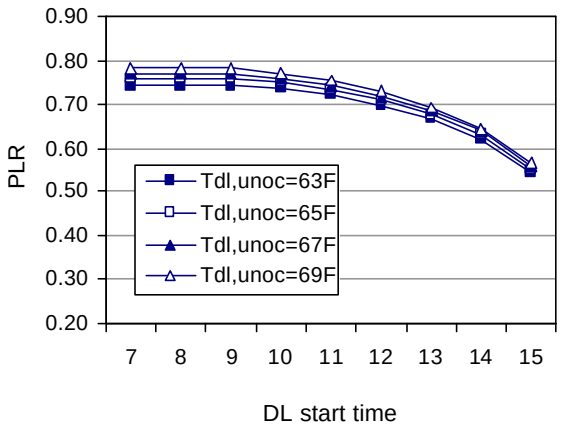

Figure 11 PLR with $T_{dl,unoc}$ varying DL start time

Figure 10 shows how *PLR* is affected by the variation of $T_{dl,oc,min}$ (set point temperature during the off-peak occupied period) under DL control. Other set point conditions were $T_{ns,unoc}$=80°F, $T_{dl,unoc}$=67°F, $T_{dl,oc,max}$=76°F and H_{pc}=12 midnight. Peak load reduction increases (*PLR* decreases) with decreasing $T_{dl,oc,min}$, with a greater impact occuring for shorter on-peak periods. The effect of DL start-time on peak load reduction becomes greater as $T_{dl,oc,min}$ is reduced. Figure 11 shows the impact of $T_{dl,unoc}$ (set point for night-precooling during the unoccupied period) on *PLR*. Other set point conditions were $T_{ns,unoc}$=80°F, $T_{dl,oc,min}$=69°F, $T_{dl,oc,max}$=76°F, and H_{pc}=12 midnight. The impact of $T_{dl,unoc}$ is small and *PLR* decreases slightly as $T_{dl,unoc}$ is lowered.

Figure 12 shows *PLR* as a function of $T_{dl,oc,max}$. Other set point conditions were $T_{ns,unoc}$=80°F, $T_{dl,unoc}$=67°F, $T_{dl,oc,min}$=69°F, and H_{pc}=12 midnight. The impact of $T_{dl,oc,max}$ on peak load reduction is greater than that of other set point temperatures under DL. As $T_{dl,oc,max}$ increases, *PLR* decreases (greater peak load reduction). *PLR* also decreases as the DL start-time increases and its impact gets larger as $T_{dl,oc,max}$ increases.

It's interesting to compare the peak load reduction of DL strategies with that associated with increasing the occupied setpoint for night setup control. Figure 13 shows the impact of $T_{ns,oc}$ on PLR_{ns}. As $T_{ns,oc}$ (set point temperature during occupied period under NS) increases, PLR_{ns} decreases about 10% compared to the peak cooling load under NS with an occupied set point temperature of 74°F. The effect on peak load reduction of raising this set point is significantly less than the effect of employing the DL control strategy.

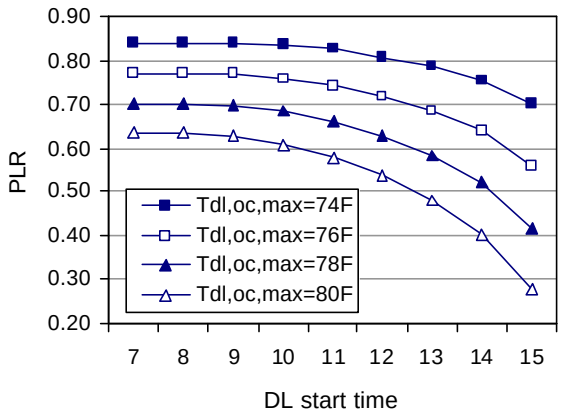

Figure 12 PLR with $T_{dl,oc,max}$ varying DL start time

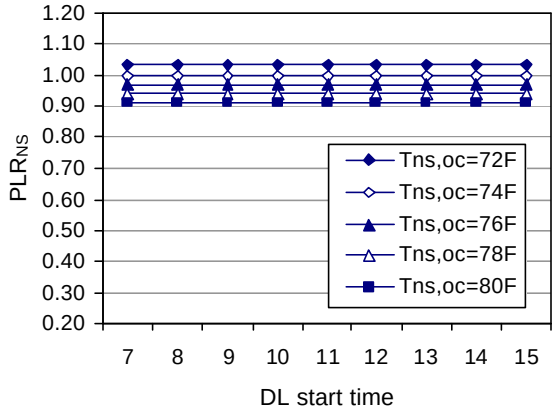

Figure 13 PLR_{ns} with $T_{ns,oc}$ varying DL start time

CONCLUSIONS

An inverse building simulation model based on a simplified thermal network was developed for a facility that is representative of small commercial buildings. The building model was then used to evaluate the potential for peak load reduction with a demand-limiting control strategy that utilizes energy storage within the building structure.

The peak demand during the on-peak period was reduced by about 25% to 45% with the demand-limiting strategy depending on the start time of the on-peak period as compared with conventional control. The potential for peak load reduction with the DL strategy increases significantly as the start of the on-peak, demand-limiting period moves to later in the day. Also, as the demand-limiting period starts later, the peak load reduction becomes more sensitive to the temperature setpoints employed prior to and during the demand-limiting period. When the demand-limiting period begins in the afternoon, demand reduction is insensitive to the amount of precooling applied in the unocuppied period.

The facility considered in this study is relatively lightweight and is representative of many small commercial buildings. Greater potential should be possible for large commercial buildings because of a smaller ratio of external area to thermal mass, the use of heavier weight materials, and the availability of more favorable electrical rate structures. However, small commercial buildings are an excellent application for use of building thermal mass because the savings are significant and they account for a significant portion of the total cooling requirements for commercial building stock. Further, it is easier to develop an intelligent controller for small commercial buildings since they typically use packaged air conditioners with a single thermostat controlling a single unit for individual zones.

NOMENCLATURE

A = coefficient matrix in the state space representation
B = coefficient matrix in the state space representation
C = capacitance (Btu/F)
C = coefficient matrix in the state space representation
DL = demand-limiting control strategy
D = coefficient matrix in the state space representation
E_{rms} = RMS error (%)
E = scalar transfer function coefficients for past histories of heat flow
H_{pc} = night precooling start time
h = convective heat transfer coefficient (Btu/hr-ft^2-F)
k_t = thermal conductivity (Btu/hr-ft-F)
N = number
NS = night-setup control strategy
PC = precooling control strategy
PLR = peak load ratio
Q = rate of heat transfer (Btu/hr)
Q_b = rate of instantaneous heat gain to the building air (Btu/hr)
$Q_{c,k}$ = calculated cooling load at time step k (Btu/hr)
$Q_{m,k}$ = measured cooling loads at time step k (Btu/hr)
$Q_{m,max}$ = maximum measured load during the testing period (Btu/hr)
R = thermal resistance (F-hr/Btu)
S = series of row vectors containing transfer function coefficients for past histories of heat flow
T = temperature (F)
t = time (hour)
u = vector of input variables
x = vector of state variables
Y = vector of output variables

Greek

τ_{eff} = effective window transmittance for solar radiation
r = density (lb/ ft^3)

Subscripts

a = ambient
b = building
dl = demand-limiting control
e = external wall
eff = effective
f = floor
g = ground
g,rad = radiative internal heat gain
g,conv = convective internal heat gain
i = internal
k = time stage
max = maximum
ns = night-setup control
oc = occupied period
op = on-peak period
r = roof and ceiling

sol	=	solar irradiative absorption	**x**	=	state variable
test	=	test period	z	=	zone
unoc	=	unoccupied period	zo	=	adjacent zone
w	=	window			

REFERENCES

Braun, J.E. 1990. "Reducing Energy Costs and Peak Electrical Demand through Optimal Control of Building Thermal Storage", ASHRAE Transactions, Vol.96, No.2, pp.839-848.

Braun, J.E., Montgomery, K.W., and Chaturvedi, N. 2001. "Evaluating the Performance of Building Thermal Mass Control Strategies", International Journal of HVAC&R Research, Vol.7, No.4, pp.403-428.

Braun, J.E., Lawrence, T.M., Klaassen, C.J., and House, J.M. 2002. "Demonstration of Load Shifting and Peak Load Reduction with Control of Building Thermal Mass", Proceeding of the 2002 ACEEE Conference on Energy Efficiency in Buildings, Monterey, CA.

Chaturvedi, N. and Braun, J.E. 2002. "An Inverse Grey-Box Model for Transient Building Load Prediction", International Journal of Heating, Ventilating, Air-Conditioning and Refrigerating Research, Vol.8, No.1, pp.73-100.

Gouda, M.M., Danaher, S., and Underwood, C.P. 2002. "Building Thermal Model Reduction Using Nonlinear Constrained Optimization", Building and Environment, Vol.37, pp.1255-1265.

Henze, G.P., Felsmann, C., and Knabe, G. 2004. "Evaluation of Optimal Control for Active and Passive Building Thermal Storage", International Journal of Thermal Sciences, Vol.43, pp.173-183.

Keeney, K.R., Braun, J.E. 1996. "A Simplified Method for Determining Optimal Cooling Control Strategies for Thermal Storage in Building Mass", International Journal of HVAC&R Research, Vol.2, No.1, pp.59-78.

Keeney, K.R. and Braun, J.E. 1997. "Application of Building Precooling to Reduce Peak Cooling Requirements", ASHRAE Transactions, Vol.103, No.1, pp.463-469.

Kintner-Meyer, M. and Emery, A.F. 1995. "Optimal Control of an HVAC System Using Cold Storage and Building Thermal Capacitance", Energy and Buildings, Vol.23, pp.19-31.

Price, B.A. and Smith, T.F. 2000. "Description of the Iowa Energy Center Energy Resource Station: Facility Update III", Technical Report ME-TFS-00-001, The University of Iowa, March 2000.

Seem, J.E., Klein, S.A., Beckman, W.A. and Mitchell, J.W. 1989. "Transfer Functions for Efficient Calculations of Multi Dimensional Heat Transfer", Journal of Heat Transfer – Transactions of the ASME, Vol.111, No.1, pp.5-12.

Thomas, H.R. and Rees, S.W. 1999. "The Thermal Performance of Ground Floor Slabs-A Full Scale In-Situ Experiment", Building and Environment, Vol.34, pp.139-164.

Travesi, J., Maxwell, G., Klaassen, C.J., and Holtz, M. 2001. "Empirical Validation of Iowa Energy Resource Station Building Energy Analysis Simulation Models", A report of Task 22, subtask A, Building energy analysis tools, IEA, June 2001.

Zhou, Z., Rees, S.W., and Thomas, H.R. 2002. "A Numerical and Experimental Investigation of Ground Heat Transfer Including Edge Insulation Effects", Building and Environment, Vol.37, pp.67-78.